

SUPPORTING INFORMATION FOR:

An Unprecedented π -Electronic Circuit Involving an Odd Number of Carbon Atoms in a Grossly Warped Non-Planar Nanographene

Sílvia Escayola,^{a,b} Albert Poater^a, Alvaro Muñoz-Castro^{*c} and Miquel Solà^{*a}

^a Institute of Computational Chemistry and Catalysis and Department of Chemistry, University of Girona, C/M. Aurèlia Capmany, 69, 17003 Girona, Spain. E-mail: miquel.sola@udg.edu.

^b Donostia International Physics Center (DIPC), Donostia, Euskadi, Spain.

^c Grupo de Química Inorgánica y Materiales Moleculares, Facultad de Ingeniería, Universidad Autónoma de Chile, El Llano Subercaseaux 2801, Santiago, Chile. E-mail: alvaro.munoz@uautonoma.cl.

Methodology and Computational Details

The geometries of the studied system have been fully optimized at the BP86-D3/TZ2P level of theory using ADF package. For the posterior aromaticity analyses we performed single point electronic corrections at the CAM-B3LYP-GD3BJ/6-311G(d,p) level of theory using Gaussian 09 rev. D01.^{1,2,3} In previous studies, Torrent-Sucarrat *et al.* proved that BP86, between other functionals, provide a very inaccurate description of the aromaticity switches in expanded porphyrins from a geometric, energetic and magnetic point of view.⁴ On the contrary, CAM-B3LYP, M05-2X, and M06-2X were a better choice for the analysis of the aromaticity using electronic indices. Moreover, CAM-B3LYP also gives good accuracy for magnetic properties according to a recent benchmark by Lehtola *et al.*⁵

For the evaluation of the aromaticity in this system, we used indicators that capture the magnetic, geometric, and electronic aspects of aromaticity. As a particular example of geometry indicator, we used the harmonic oscillator model of aromaticity (HOMA).⁶ As magnetically based index we used the gauge-including magnetically induced current (GIMIC) method.⁷ Moreover, several electronic indices were used, including fluctuation index (FLU), multicenter indices (MCI and AV_{min}) and electron density of delocalized bonds (EDDB).^{8,9,10,11,12}

The analysis of the magnetically induced current densities was carried out by means of the GIMIC program available at GitHub (<https://gimic.readthedocs.io>). The one-electron density matrix, the magnetically perturbed one-electron matrices and basis set data required for the GIMIC calculation were obtained from an NMR shielding calculation (NMR=GIAO) performed with Gaussian 09 rev. D.01. For the GIMIC calculation we have to set the following parameters: integration plane, orientation of the magnetic field, dimensions of the cube (volume in which the calculation is done, defined by the origin and length) and the grid spacing. In the particular case of the planar structure is easy to choose the magnetic field orientation perpendicular to the molecular plane. The molecular plane has been chosen to be the xy (ivect=[1,0,0] and jvect=[0,1,0]), thus the magnetic goes in the z direction. The grid origin, spacing of the points, and cube length and have been defined as [-20.0, -20.0, -20.0], [0.5, 0.5, 0.5] and [40.0, 40.0, 40.0] (in bohr), respectively. In the non-planar system, the selection of the magnetic field orientation is not straightforward. Therefore, we used different orientations of the magnetic field (Figure S1) to estimate the aromaticity of the system.

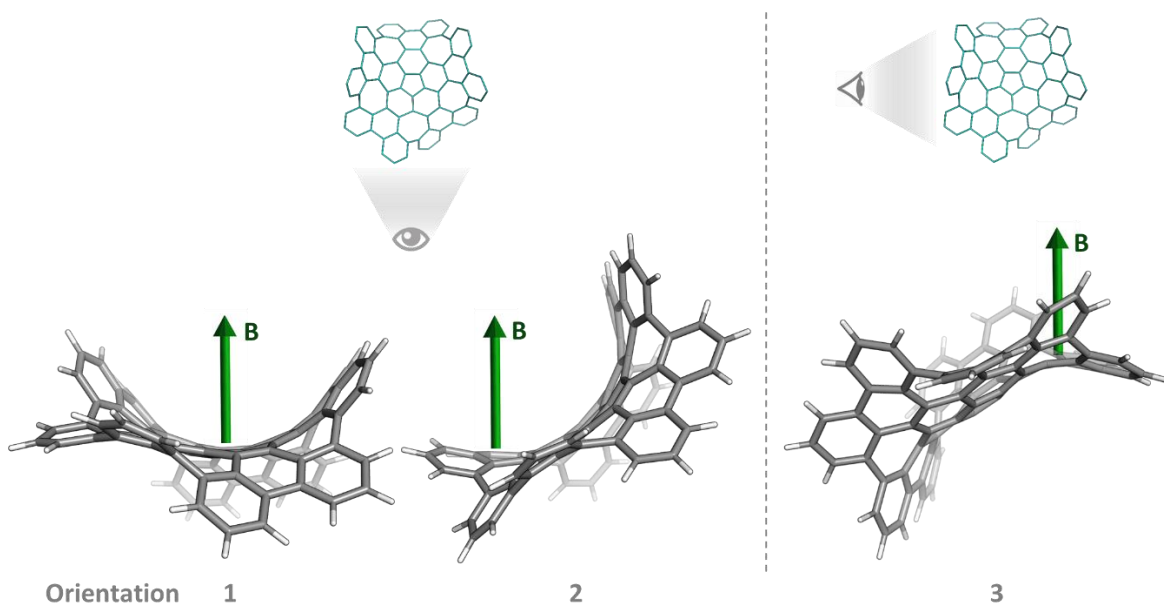


Figure S1. Different orientations of the magnetic field vector (B) with respect the molecular structure of the PMPMP-isomer of nanographene.

MCI indices have been obtained using AIMAll together with ESI-3D packages.^{13,14,15,16} First, the AIMAll software was used to perform the QTAIM atomic partitioning to get the atomic overlap matrices and then, we used this data together with the molecular coordinates as input for the ESI-3D code to get all the above mentioned indices as well as the HOMA geometrical index. Finally, The EDDB results were computed using NBO 6.0 software coupled to the Gaussian 09 rev. D.01 version to first obtain the natural atomic orbitals (NAO) and then running the program available at <http://www.eddb.pl/runeddb/>.^{17,18} The EDDB(r) isosurfaces were generated using the Formchk and Cubegen tools from Gaussian 09 rev. D.01 package.

For the generation of EDDB(r) plots we used the Avogadro1.0 molecular editor.¹⁹ The streamline (spaghetti) plots and the line integral convolution on a surface (LIC), representing the current-density vector field, obtained with GIMIC were visualized using ParaView 5.2.0.²⁰ Finally, for the schemes and the system pictures we used ChemDraw Professional 15.0, PyMOL, and Chemcraft 1.7 programs.^{21,22,23}

The nuclear and nucleus-independent shielding tensors²⁴⁻²⁶ were calculated within the gauge-including atomic orbitals (GIAO)²⁷⁻³⁰ with the exchange expression proposed by Handy and Cohen,³¹ the correlation expression proposed by Perdew, Burke, and Ernzerhof³² (OPBE), and an all-electron STO-TZ2P basis set. The OPBE functional gives good results for the ^{13}C NMR shielding constants, referenced to TMS as $^{13}\text{C}\delta = \sigma^{\text{TMS}} - {}^{\text{C}}\sigma$ (^{13}C -NMR $\sigma^{\text{TMS}}=192.34$ ppm).³³ To evaluate the magnetic response or induced field (B^{ind}), upon an external magnetic field (B^{ext}) at the molecular surroundings, a map representation of the nucleus independent shielding tensor (σ_{ij}) was obtained, where $B_i^{\text{ind}} = -\sigma_{ij}B_j^{\text{ext}}$.^{24,26,34-36} For convenience, the i and j suffixes are related to the x-, y- and z-axes of the molecule-fixed Cartesian system ($i,j = x,y,z$).

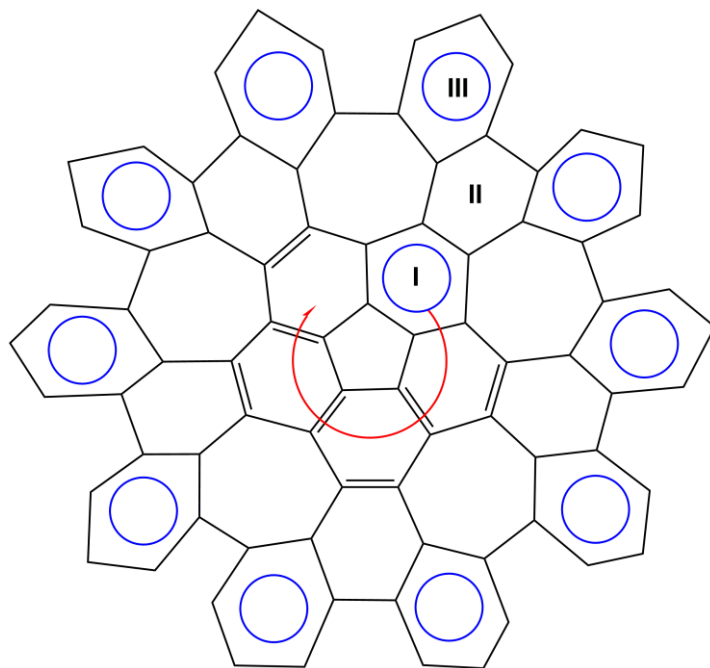


Figure S2. The Clar structure of $C_{80}H_{30}$ nanographene with 80π -electrons (60π -electrons in rings III and 20π -electrons in the corannulene core).

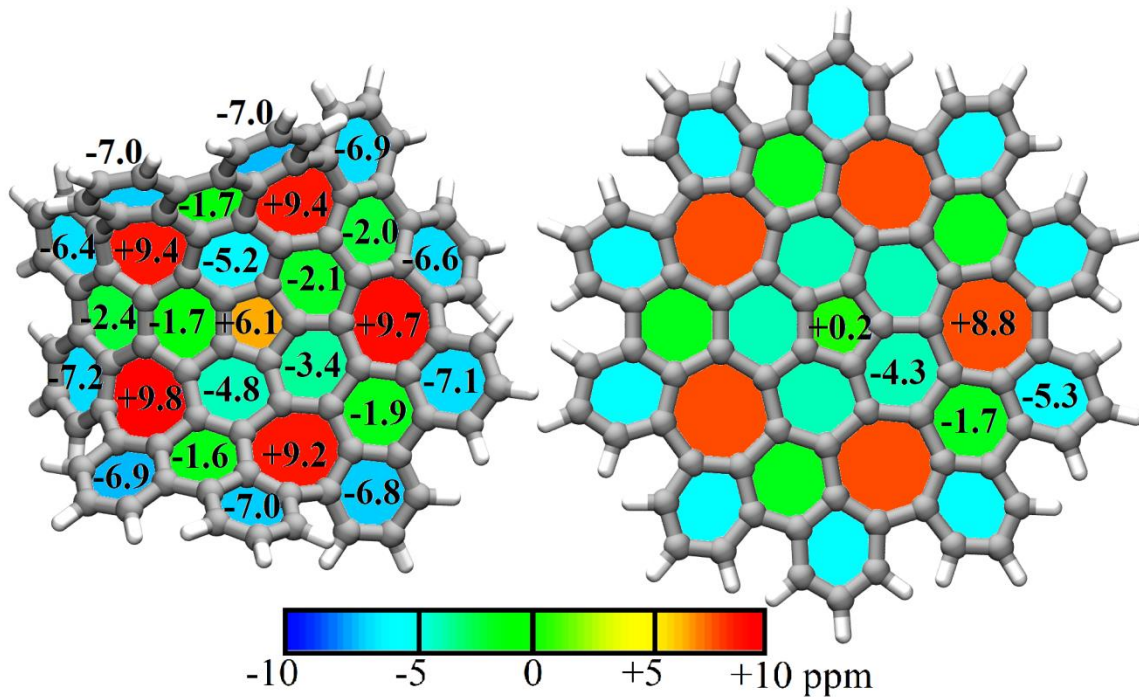


Figure S3. NICS(0) values for each ring for $C_{80}H_{30}$ nanographene (left), and its planar counterpart (right), denoting the local aromatic character of each ring.

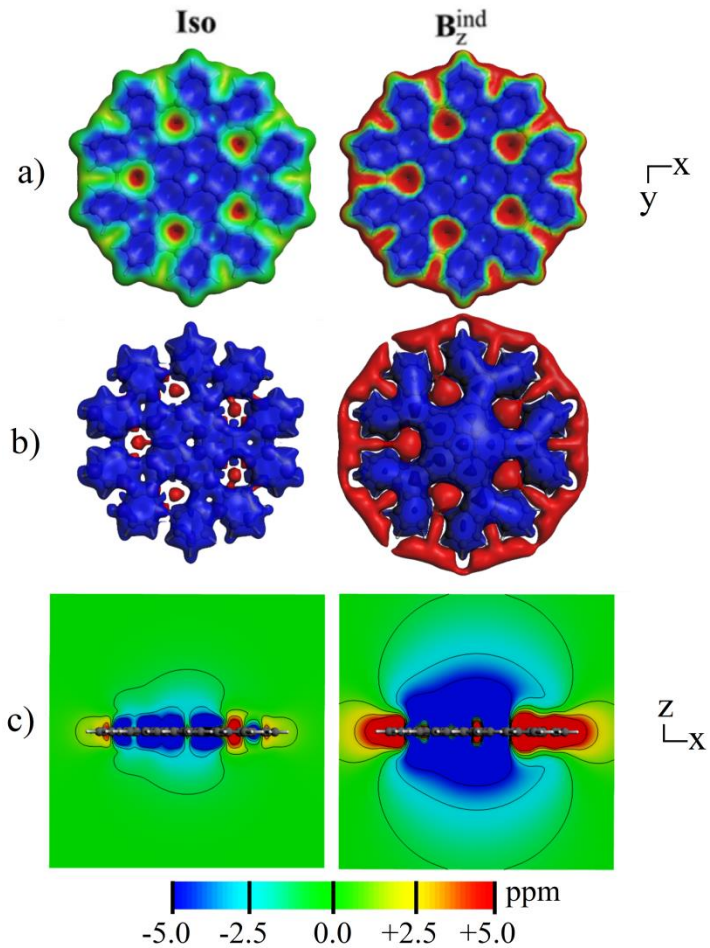


Figure S4. Induced magnetic field for the planar nanographene, drawn over 0.01 a.u. electron density isosurface (a), shielding and deshielding isosurface at ± 5.0 ppm (b), and as a cutplane over the xz-plane (c). Blue: Shielding; Red: Deshielding.

Reference molecules

For having reference aromaticity values we choose molecules that have been clearly assigned as aromatic, antiaromatic or non-aromatic. We selected benzene, cyclobutadiene and cyclohexane (chair conformation) as references for aromatic, antiaromatic and non-aromatic compounds, respectively.

The results of the aromaticity indices can be interpreted as it is explained in the following lines. In the case of MCI high positive values (close to those obtained for benzene) are indicative aromatic character, whereas smaller values (close to cyclohexane and cyclobutadiene) correspond to non-aromatic species (Table S1). In the case of indices based on references (HOMA and FLU), the maximum aromaticity is achieved when the system resembles more the references molecules, *i.e.* benzene for C-C bonds. In the case of FLU, the closer the value to zero, the more aromatic the compound is. In the case of HOMA the maximum aromaticity is achieved for values close to 1.

Table S1. Aromaticity results according to FLU, HOMA, and MCI for reference systems calculated at the CAM-B3LYP-GD3BJ/6-311G(d,p)//BP86-D3/TZ2P level of theory.

molecule	FLU	HOMA	MCI	$MCI^{1/N}$
C_6H_6	0.000	0.979	0.0729	0.646
C_4H_4	0.103	-4.141	0.0089	0.307
C_6H_{12}	0.090	-4.627	0.0003	0.259

For the magnetic-based index, GIMIC (Figure S5 and Table S2), the aromatic or antiaromatic character is given by the direction of the net current flow. According to the convention, the current flowing clockwise is known as diatropic (and its integrated current density is positive), while a counterclockwise current is paratropic (the integrated current density is negative). In the current density plots, the intensity of the current decreases going from white ($0.4 \text{ nA}\cdot\text{T}^{-1}\cdot\text{\AA}^{-2}$) or light yellow to red and the black ($4\cdot10^{-5} \text{ nA}\cdot\text{T}^{-1}\cdot\text{\AA}^{-2}$), and the black arrows indicate the direction of the current flow. The current strength is computed as the integral of the current density susceptibility in a plane perpendicularly to a selected bond. In the case of non-aromatic compounds, we expect to observe discontinuous currents or diatropic and paratropic currents that cancel each other.

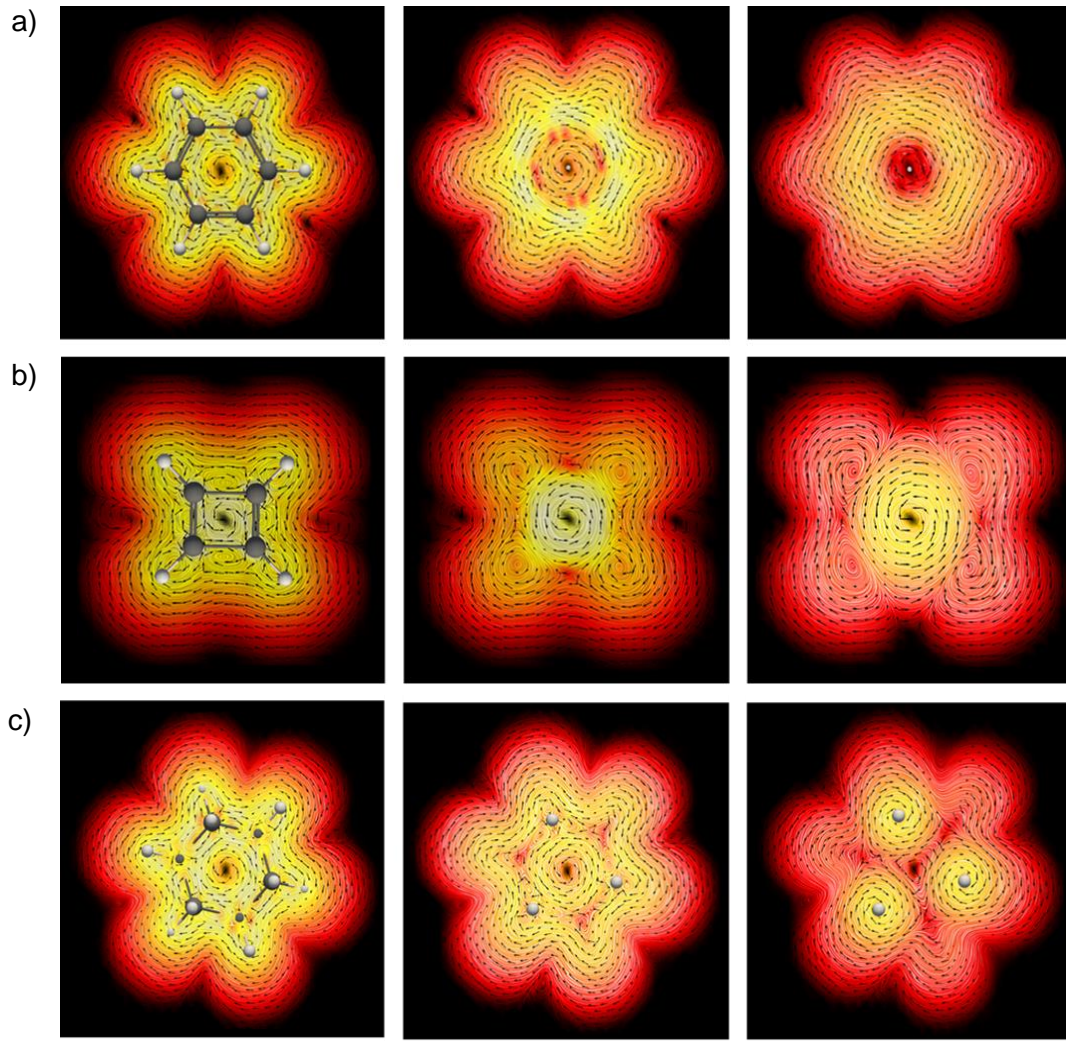


Figure S5. Representation of the current density using the line integral convolution (LIC) for a) benzene, b) cyclobutadiene and c) cyclohexane systems. Top view of the currents in the molecular plane (0 bohr) and the parallel planes located at 1 and 2 bohr (from left to right, respectively).

Table S2. Ring current strengths dissected in diatropic and paratropic contributions (in nA/T) for benzene, cyclobutadiene and cyclohexane systems.

molecule	diatropic	paratropic	Net current strength
C₆H₆	16.23	-3.92	12.31
C₄H₄	3.86	-24.81	-20.95
C₆H₁₂	6.13	-5.26	0.87

Finally, from the EDDB analysis we obtain the isosurfaces and the number of delocalized electrons. We computed the $\text{EDDB}_G(\mathbf{r})$ and $\text{EDDB}_H(\mathbf{r})$ functions, where G stands for global and H is the EDDB index without taking into account the H atoms. We will use also the $\text{EDDB}_P(\mathbf{r})$ for computing the electron delocalization in a selected pathway. In the case of having delocalized electrons we will observe a continuous thick surface, while in the case of non-aromatic (poor delocalization) this surface will disappear or have discontinuities (Figure S6). Alternatively, with the number of

delocalized electrons together with the Hückel and Baird rules we can determine the aromatic character of the system, *e.g.* for benzene we expect 6 delocalized electrons.

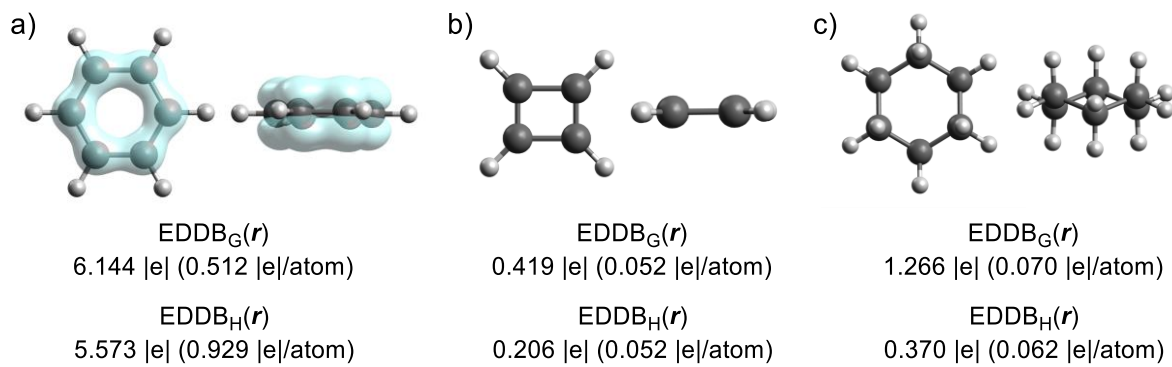


Figure S6. Representation of the $\text{EDDB}_G(r)$ isosurfaces using an isocontour of 0.02, and $\text{EDDB}_G(r)$ and $\text{EDDB}_H(r)$ values for a) benzene, b) cyclobutadiene and c) cyclohexane systems.

Studied nanographene

EDDB isosurfaces

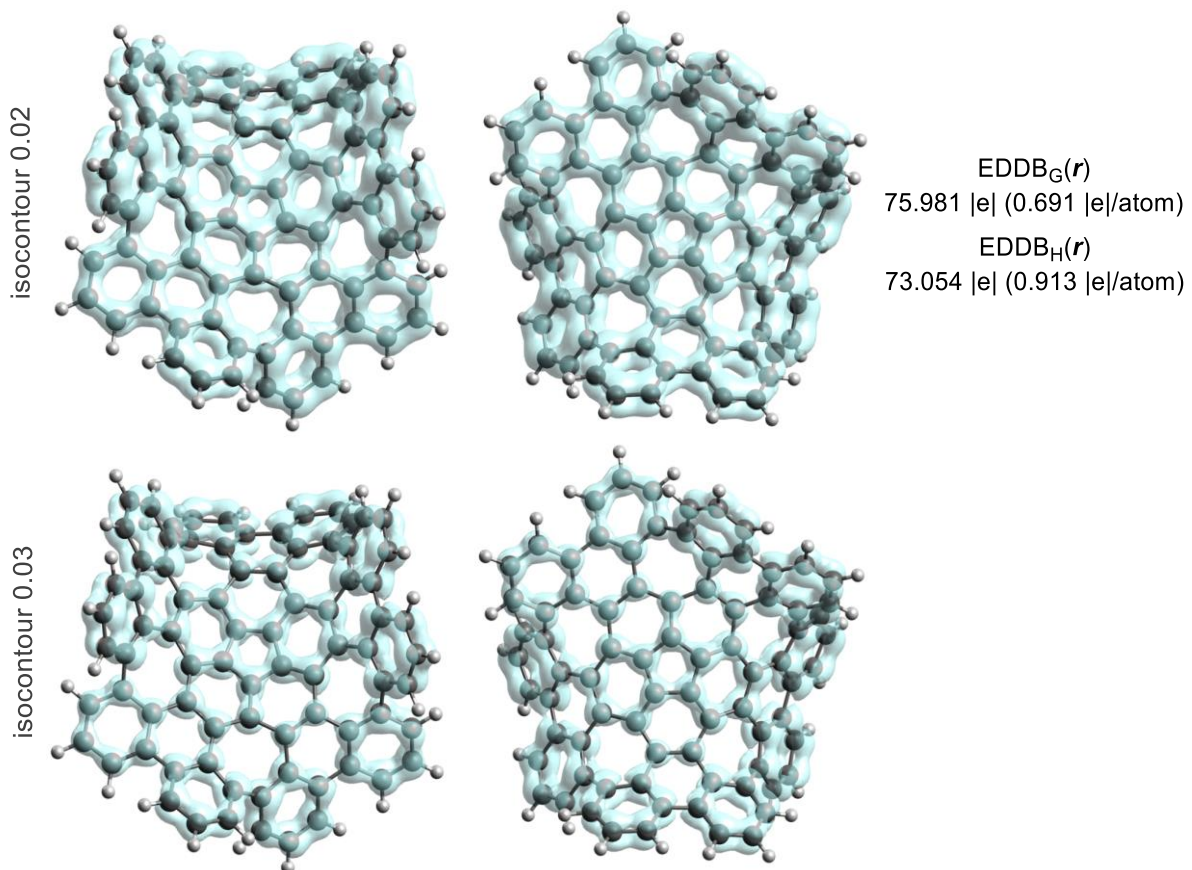


Figure S7. Representation of the $\text{EDDB}_G(r)$ isosurfaces using an isocontour of 0.02 and 0.03 (two different views from the top), and $\text{EDDB}_G(r)$ and $\text{EDDB}_H(r)$ values for the PMPMP-isomer of the nanographene.

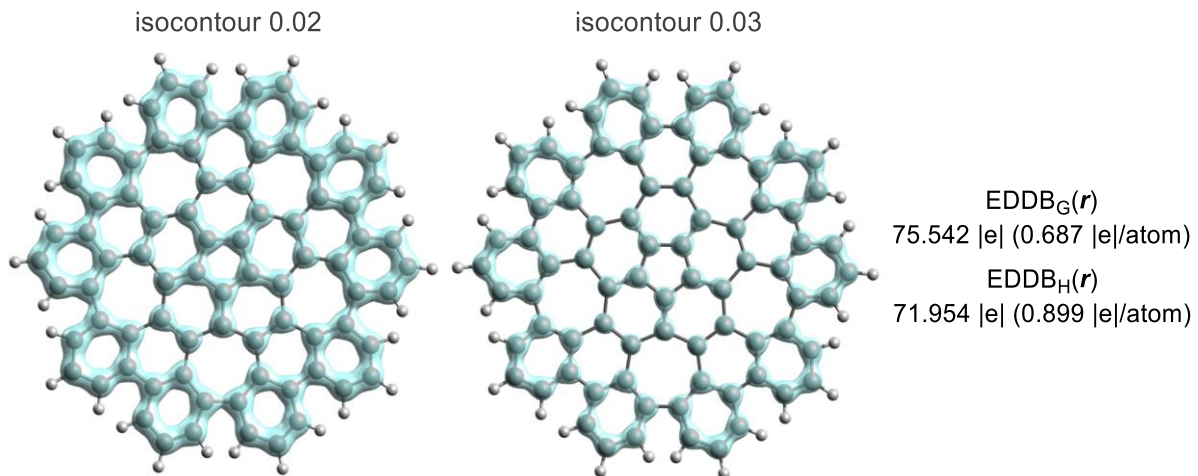


Figure S8. Representation of the $\text{EDDB}_G(r)$ isosurfaces using an isocontour of 0.02 and 0.03, and $\text{EDDB}_G(r)$ and $\text{EDDB}_H(r)$ values for the planar form of the nanographene.

GIMIC Results - Current Density Pathways and Current Strengths

In the case of the warped $C_{80}H_{30}$ nanographene the quantification of the aromaticity of the different pathways by means of the integrated current strength could not be done. This is because the distorted geometry, far from the planarity, hampers the reliable definition of the integration planes. However, this does not prevent us to perform the measures in the case of the planar nanographene where we were able to perform these measures (Figure S9).

If we analyse the integrated current strengths of the bonds forming each of the pathways, on the one hand, we observe that in the 50-electron pathway most of the values range from 11.2 to 8.5 $nA \cdot T^{-1}$, but we also find 5 bonds with a small negative current ($-1.2 nA \cdot T^{-1}$), corresponding to the external bond of the 7-MRs. On the other hand, the 75-electron pathway has only positive current strengths and these range from 11.2 to 8.5 $nA \cdot T^{-1}$. This is an indicative that the 75-electron is more aromatic than the 50-electron pathway, in good agreement with $\text{EDDB}_P(r)$ results.

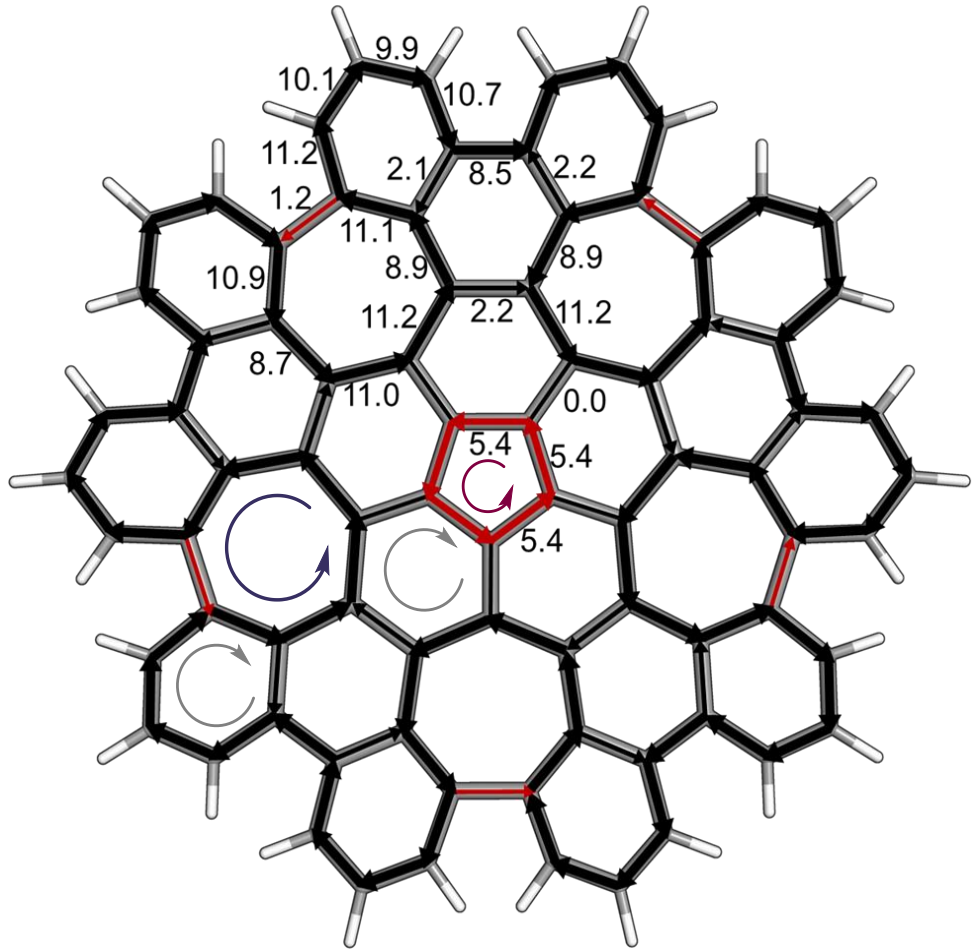


Figure S9. Calculated net current strengths (in $\text{nA}\cdot\text{T}^{-1}$) passing through the selected bonds in planar nanographene.

Then, to have a clear picture of the current density we plot the current density streamlines directly (shown in Figure 4 in the manuscript for planar and S11 for warped nanographene) and by means of the line integral convolution (LIC) technique (Figures S12-15).

For the representation of the streamlines, we defined the magnetic field in the negative Z direction. Then, using ParaView program,²⁰ mentioned above in the computational details, we visualized the molecule oriented towards the negative Z axis and we set the integration direction as forward. Using the stream tracer tool, a sphere with a radius of 1 bohr, and a value of 120 as the length of the field line, we obtained the streamline plot. For the identification of the possible circuits, we placed the sphere at the plane 1.8897 bohr (1 Å) above the molecular plane and we displaced the sphere from centre of the 5-MR to the external part of the molecule, as shown in Figure S10.

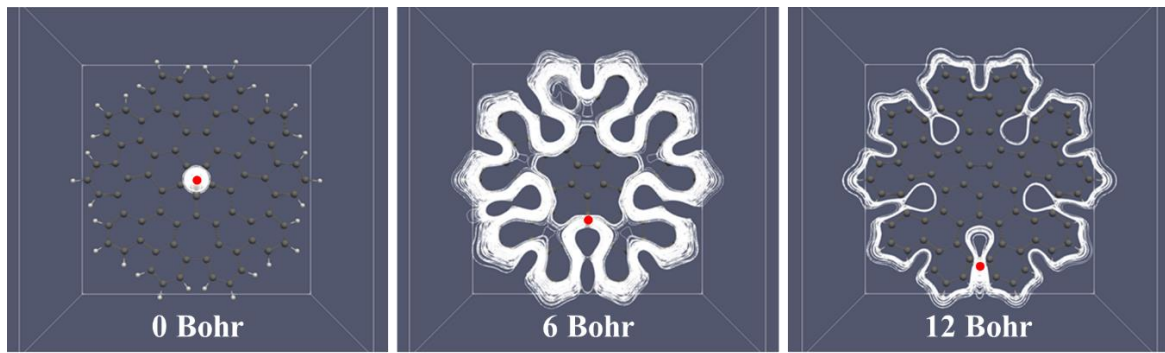


Figure S10. Streamline representation of the current density placing the sphere at 0, 6, and 12 bohrs from the central ring. In all cases, the sphere is located in the plane at 1.89 bohr above the molecule.

We observed that for most of the positions tested, we found the 75-electron pathway (also identified using other indices). In the particular case of the streamline represented in Figure 4, the sphere was located at 12 bohr from the centre and contained at the plane at 1 Å above the molecular plane.

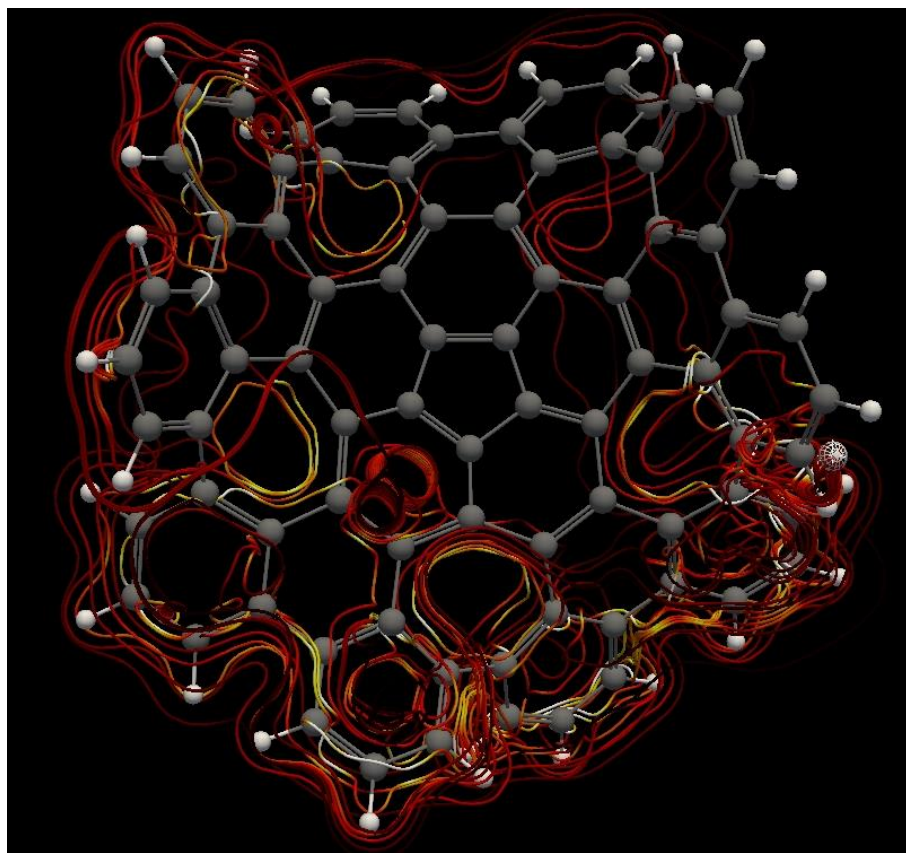


Figure S11. Stream line representation of the current density in PMPMP- isomer of nanographene. The intensity of the current decreases going from white ($0.1 \text{ nA} \cdot \text{T}^{-1} \cdot \text{bohr}^{-2}$), light yellow, red to black ($1 \cdot 10^{-6} \text{ nA} \cdot \text{T}^{-1} \cdot \text{bohr}^{-2}$).

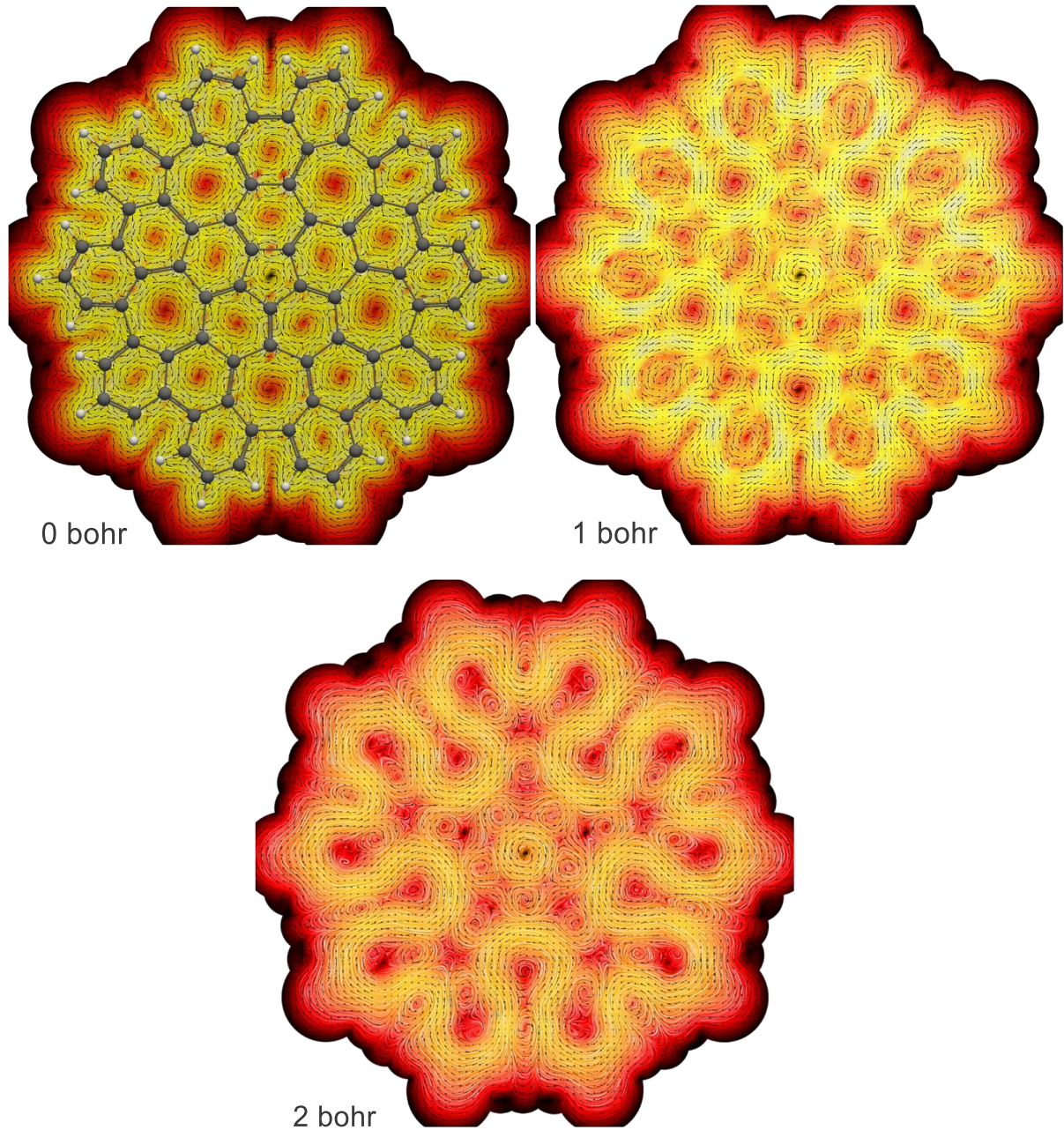


Figure S12. Current density in planar nanographene in the molecular plane, and the planes at 1 and 2 bohr above the molecular plane.

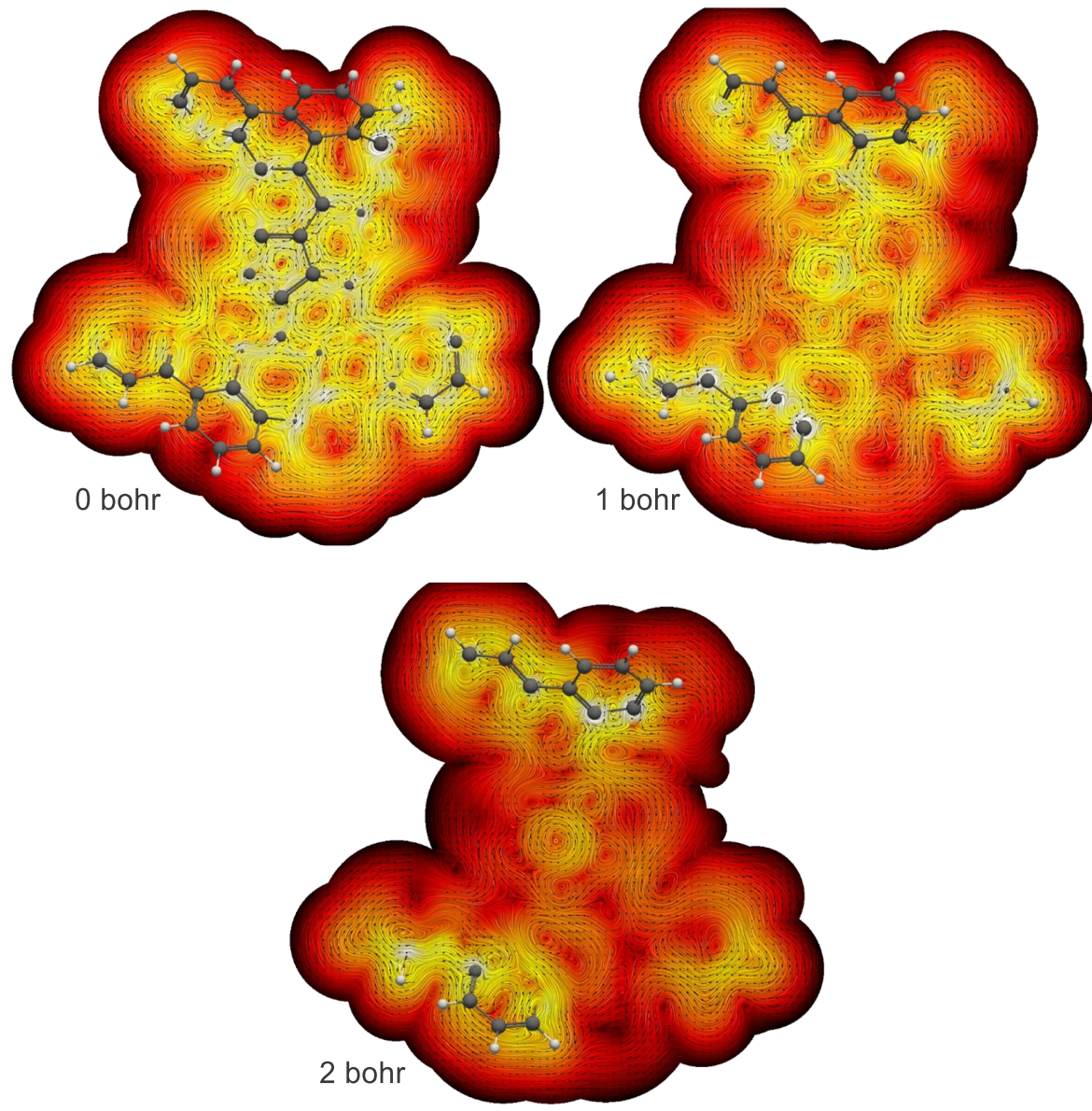


Figure S13. Current density in PMPMP isomer of nanographene in the molecular plane, and the planes at 1 and 2 bohr above the molecular plane. The magnetic field is placed as in orientation 1, represented in Figure 2.

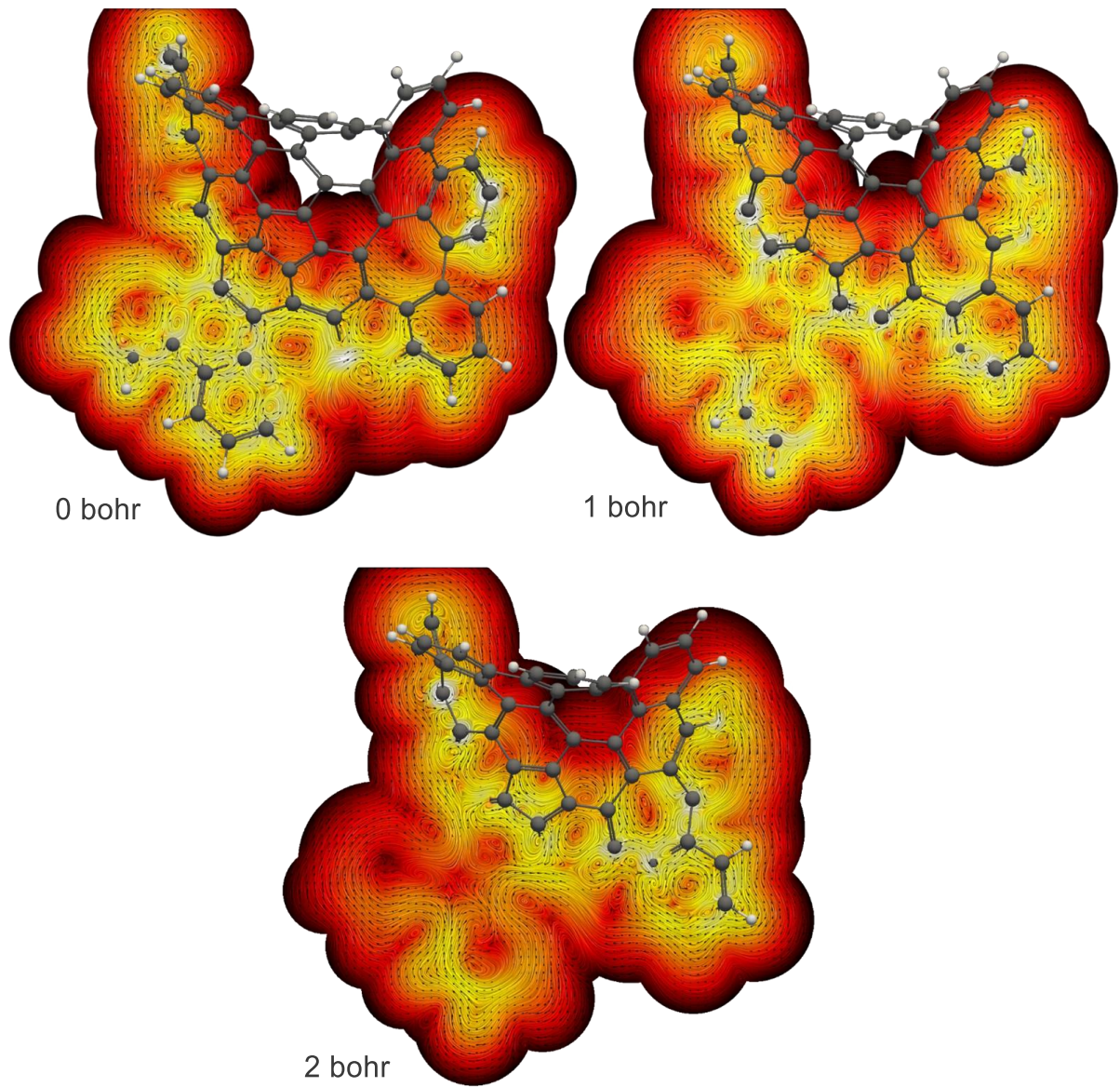


Figure S14. Current density in *PMPMP*-isomer of nanographene in the molecular plane, and the planes at 1 and 2 bohr above the molecular plane. The magnetic field is placed as in orientation 2, represented in Figure 2.

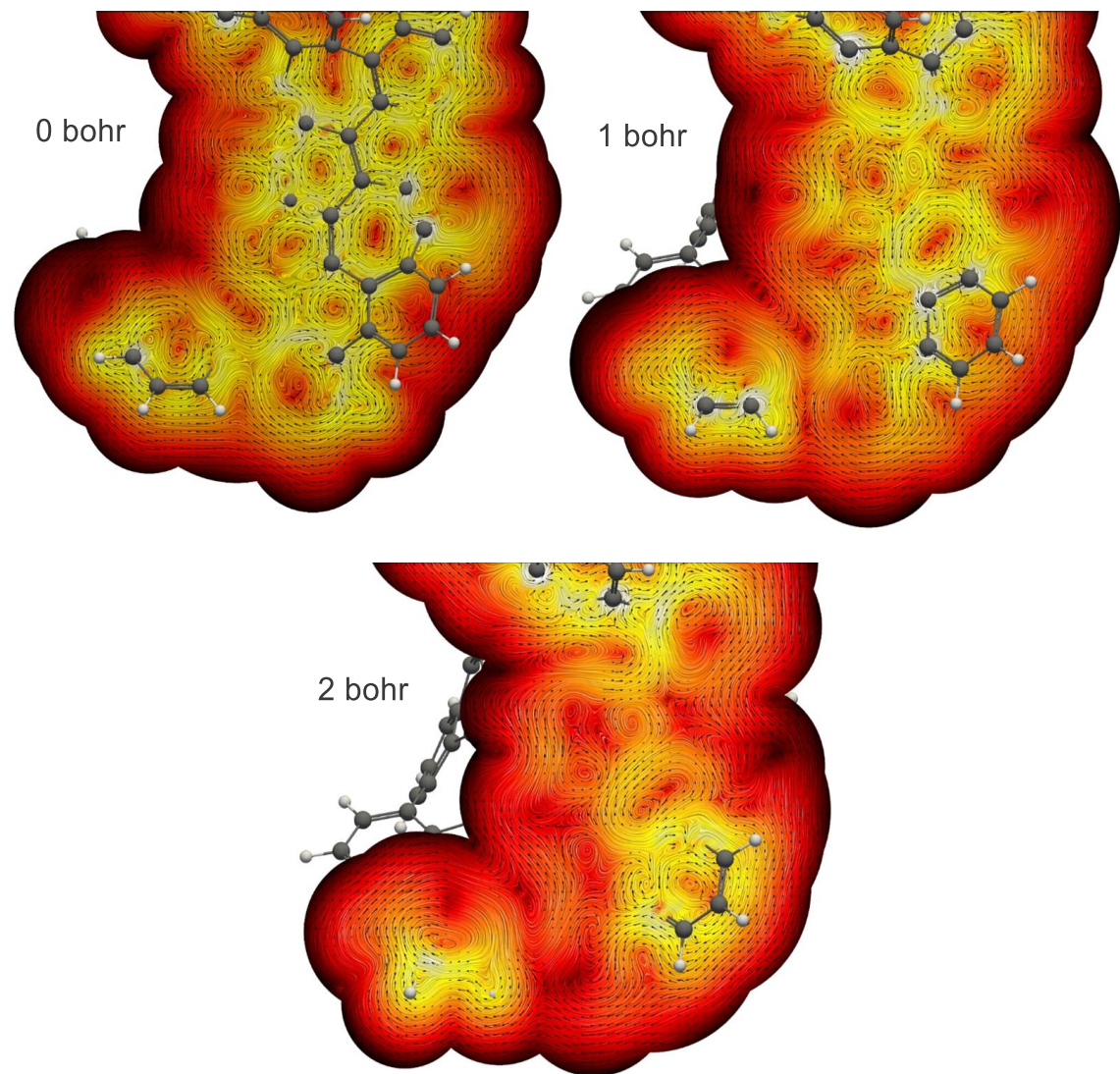


Figure S15. Current density in *PMPMP*-isomer of nanographene in the molecular plane, and the planes at 1 and 2 bohr above the molecular plane. The magnetic field is placed as in orientation 3, represented in Figure 2.

Local Aromatic Descriptors

The characteristic of each ring type (Figure S16) is evaluated via FLU, HOMA, and MCI indices. The obtained results show external hexagons (**III** to **III''''**) as the most locally aromatic rings with similar C-C distances (HOMA, Table S3), leaving the remaining 6-MRs of type **II** and **I**, to be of lesser aromatic characteristics. This result agrees with the Clar structure of $C_{80}H_{30}$ nanographene shown in Figure S2.

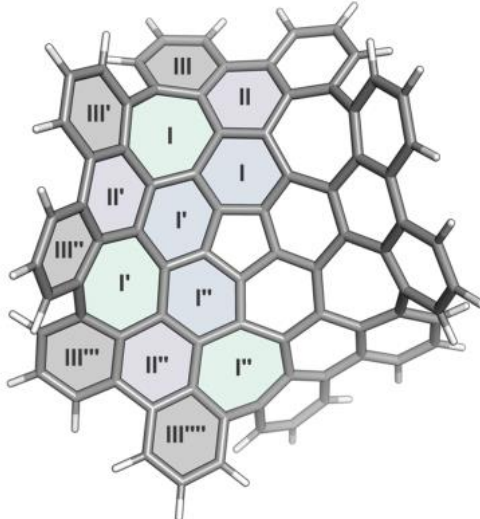


Figure S16. Representation of different 6-MR and 7-MR in PMPMP-isomer of nanographene **1**.

For all indices of aromaticity, rings **III**, which have a π -sextet fully localized in the ring (Figure 6), are the most aromatic ones. Rings **II**, as well as the 5-MR and the 7-MRs, are empty rings according to Clar's nomenclature and, consequently, they are predicted to be non-aromatic. The paratropic behavior of 5- and 7-MRs is likely due to the diatropic rings present in the adjacent 6-MRs, like in corannulene and coronene.^{37,38} Finally, the five 6-MRs **I** share a migrating π -sextet resulting in a minor aromatic character. HOMA values indicating that 5-MRs are aromatic and 7-MRs are antiaromatic and pointing out that rings **II** are more aromatic than rings **I** are not reliable. The reason for the HOMA failure in this nanographene, especially in the planar structure, is the highly strained structure that results from the presence of 5- and 7-MRs. As found in previous works, deviation from planarity leads to relatively small changes in the cyclic π -electron delocalization of the $C_{80}H_{30}$ nanographene.^{39,40} There are two interesting motifs in its structure. On the one hand, the 5-MR and the five adjacent 6-MR have a similar aromatic behavior to that of corannulene, although with some lower aromaticity of the 6-MRs. This corannulene ring has the typical radial structure that avoids double bonds in [5,6] bonds like in C_{60} , where [5,6] bonds are larger (exp. 1.410 Å av.) than [6,6] bonds (exp. 1.356 Å av.). One the other hand, **I**, **II**, and two **III** vicinal 6-MRs have a structure with an aromatic character that resembles that of triphenylene, with rings **I** and **III** much more aromatic than the central ring **II**. The trends remain the same in the planar structure of the $C_{80}H_{30}$ nanographene. For comparison purposes, Figures S5 and S6 and Tables S1 and S2 gather reference aromaticity values for monocyclic conjugated molecules that have a clear aromatic (benzene), antiaromatic (cyclobutadiene) or non-aromatic (cyclohexane, chair conformation) character.

Table S3. Aromaticity results of the small ring (5-MR, 6-MRs and 7-MRs, represented in Figure S16) moieties according to FLU, HOMA, and MCI in *PMPMP*-isomer of the C₈₀H₃₀ nanographene.^a

<i>PMPMP</i>-isomer	FLU	HOMA	MCI	MCI^{1/N}
5-MR	0.033	0.870	0.0106	0.4029
6-MR I	0.013	0.383	0.0223	0.5307
6-MR I'	0.020	0.054	0.0150	0.4965
6-MR I''	0.017	-0.094	0.0185	0.5141
6-MR II	0.023	0.135	0.0098	0.4624
6-MR II'	0.022	0.254	0.0110	0.4717
6-MR II''	0.020	0.125	0.0121	0.4793
6-MR III	0.004	0.866	0.0471	0.6009
6-MR III'	0.004	0.882	0.0471	0.6010
6-MR III''	0.004	0.869	0.0457	0.5979
6-MR III'''	0.005	0.844	0.0438	0.5937
6-MR III''''	0.005	0.862	0.0432	0.5923
7-MR I	0.033	-0.202	0.0014	0.3900
7-MR I'	0.033	-0.420	0.0014	0.3908
7-MR I''	0.031	-0.480	0.0016	0.3981
Planar structure	FLU	HOMA	MCI	MCI^{1/N}
5-MR	0.037	-1.914	0.0103	0.4008
6-MR I	0.020	-4.798	0.0200	0.5208
6-MR II	0.024	-3.589	0.0115	0.4752
6-MR III	0.005	0.150	0.0454	0.5973
7-MR	0.036	-5.947	0.0016	0.3970

^a See Table S1 for FLU, HOMA, and MCI values in selected reference molecules.

Table S4. Cartesian coordinates of the optimized and planar *PMPMP*.

Warped C₈₀H₃₀ nanographene, optimized at BP86-D3/TZ2P level of theory:

110

Warped nanographene SCF Energy: -3065.80675824 A.U.

C	-0.966715	0.706570	0.053386
C	-0.961350	-0.691067	-0.148593
C	0.369797	-1.142143	-0.086403
C	1.200320	0.000000	0.010137
C	0.357948	1.126640	0.171473
C	-2.062428	1.431889	0.446251
C	-3.309484	0.720686	0.114374
C	-3.310202	-0.672710	-0.183244
C	-2.073404	-1.478611	-0.065998
C	-1.775348	-2.867665	0.222946
C	-0.412483	-3.321904	0.453203
C	0.759377	-2.431088	0.211056
C	2.239971	-2.538021	0.334575
C	3.115907	-1.362188	0.241201

C	2.556401	0.000000	0.189176
C	3.071713	1.401064	0.258009
C	2.205191	2.497342	0.586373
C	0.748679	2.326536	0.708497
C	-0.354185	3.094656	1.288830
C	-1.727342	2.664006	1.146076
C	-4.467202	1.515646	-0.246963
C	-4.712113	2.784348	0.339506
C	-5.671311	3.626466	-0.228160
H	-5.832628	4.610415	0.211685
C	-6.435224	3.217959	-1.326615
H	-7.169728	3.895211	-1.761629
C	-6.292084	1.932501	-1.818503
H	-6.951603	1.595957	-2.615295
C	-5.328802	1.053038	-1.281273
C	-4.403829	-1.219530	-0.959805
C	-5.244634	-0.337810	-1.696618
C	-6.013029	-0.855467	-2.760956
H	-6.607813	-0.184645	-3.377072
C	-6.014772	-2.210285	-3.043279
H	-6.580273	-2.594611	-3.891783
C	-5.339428	-3.093042	-2.191189
H	-5.425271	-4.169343	-2.339643
C	-4.571832	-2.620842	-1.125995
C	-2.898425	-3.752216	0.517464
C	-4.187512	-3.588473	-0.067491
C	-5.242275	-4.410101	0.352044
H	-6.228879	-4.248507	-0.080112
C	-5.064379	-5.408140	1.310418
H	-5.903778	-6.032674	1.614788
C	-3.807319	-5.610740	1.843552
H	-3.652036	-6.431033	2.540020
C	-2.719075	-4.803829	1.453256
C	-0.265788	-4.554085	1.219318
C	-1.381487	-5.105176	1.918124
C	-1.179797	-6.003541	2.985732
H	-2.028535	-6.319072	3.587994
C	0.081450	-6.477576	3.288601
H	0.242467	-7.138168	4.139697
C	1.140553	-6.128843	2.449779
H	2.130080	-6.553442	2.614383
C	0.975584	-5.210170	1.404048
C	2.868285	-3.850058	0.364195
C	2.159540	-5.075666	0.536152
C	2.739911	-6.283545	0.139967
H	2.141623	-7.190992	0.216452
C	4.073294	-6.352665	-0.278282
H	4.497363	-7.288970	-0.638975

C	4.855288	-5.223840	-0.133108
H	5.921398	-5.260762	-0.349859
C	4.273026	-3.990405	0.234892
C	4.557737	-1.549179	0.342864
C	5.106585	-2.848117	0.502575
C	6.435098	-3.042671	0.938883
H	6.774651	-4.050991	1.168755
C	7.265561	-1.960408	1.149484
H	8.261595	-2.087566	1.571732
C	6.818557	-0.701693	0.738896
H	7.500157	0.147930	0.752129
C	5.520515	-0.494774	0.256375
C	4.354908	1.720309	-0.345810
C	5.367905	0.748380	-0.529476
C	6.391792	0.979522	-1.456719
H	7.118927	0.188707	-1.636149
C	6.486857	2.185603	-2.153852
H	7.264590	2.328301	-2.903170
C	5.610895	3.207118	-1.841862
H	5.726538	4.171730	-2.329717
C	4.571541	3.013526	-0.909272
C	2.694423	3.860359	0.450196
C	3.764714	4.124881	-0.444872
C	4.074712	5.458238	-0.787424
H	4.887955	5.667882	-1.477710
C	3.383720	6.516012	-0.227451
H	3.620923	7.541742	-0.508394
C	2.413507	6.260785	0.745622
H	1.910031	7.088651	1.244384
C	2.077959	4.954583	1.110655
C	-0.052023	4.127747	2.269440
C	1.186378	4.824080	2.286908
C	1.550875	5.568026	3.412156
H	2.521914	6.062445	3.419592
C	0.693988	5.689323	4.508444
H	1.007325	6.242201	5.393447
C	-0.576385	5.149681	4.431832
H	-1.265382	5.315991	5.255977
C	-0.988764	4.406553	3.306042
C	-2.757940	3.308175	1.950517
C	-2.377794	4.006887	3.132858
C	-3.365338	4.386645	4.065805
H	-3.080500	4.885735	4.988324
C	-4.706145	4.161195	3.819584
H	-5.458606	4.442497	4.555715
C	-5.090382	3.612990	2.594277
H	-6.147723	3.490058	2.361442
C	-4.145306	3.205154	1.646913

Planar C₈₀H₃₀ nanographene, optimized at BP86-D3/TZ2P level of theory

110

Planar nanographene SCF Energy: -3064.62905376 A.U.

C	-1.271166	0.000000	0.000000
C	-2.719906	0.000000	0.000000
C	-3.344957	-1.474582	0.000000
C	-2.436059	-2.725573	0.000000
C	-0.840497	-2.586784	0.000000
C	-4.899694	-1.707643	0.000000
C	-6.027528	-0.751703	0.000000
C	-7.375699	-1.238507	0.000000
H	-8.239737	-0.611889	0.000000
C	-7.844840	-2.523805	0.000000
H	-8.912167	-2.776483	0.000000
C	-6.838287	-3.426039	0.000000
H	-7.211836	-4.432932	0.000000
C	-5.445773	-3.061929	0.000000
C	-3.138154	-4.132195	0.000000
C	-4.594904	-4.233050	0.000000
C	-5.371504	-5.444893	0.000000
H	-6.444549	-5.489013	0.000000
C	-4.824470	-6.680988	0.000000
H	-5.394603	-7.617994	0.000000
C	-3.457107	-6.631987	0.000000
H	-3.128159	-7.647371	0.000000
C	-2.577521	-5.500231	0.000000
C	1.028395	-0.747173	0.000000
C	-0.392812	-1.208951	0.000000
C	3.572865	-0.773155	0.000000
C	2.200450	-1.598721	0.000000
C	1.839390	-3.159078	0.000000
C	0.368762	-3.636914	0.000000
C	4.967664	-1.498456	0.000000
C	6.205480	-0.723793	0.000000
C	7.546065	-1.247720	0.000000
H	8.440110	-0.652694	0.000000
C	7.830064	-2.569281	0.000000
H	8.842070	-2.992219	0.000000
C	6.695042	-3.333354	0.000000
H	7.025746	-4.348167	0.000000
C	5.318213	-2.934751	0.000000
C	2.960208	-4.261481	0.000000
C	4.434532	-4.151033	0.000000
C	5.239089	-5.337300	0.000000
H	6.306428	-5.338224	0.000000
C	4.863154	-6.652882	0.000000

H	5.578119	-7.484662	0.000000
C	3.518515	-6.791168	0.000000
H	3.228886	-7.825328	0.000000
C	2.605967	-5.678098	0.000000
C	0.109976	-5.187577	0.000000
C	1.229231	-6.125426	0.000000
C	1.145210	-7.562301	0.000000
H	1.987389	-8.228715	0.000000
C	-0.023908	-8.240785	0.000000
H	-0.113419	-9.333955	0.000000
C	-1.101326	-7.397426	0.000000
H	-1.964278	-8.025539	0.000000
C	-1.147696	-5.964809	0.000000
C	-3.344957	1.474582	0.000000
C	-2.436059	2.725573	0.000000
C	-0.840497	2.586784	0.000000
C	-4.899694	1.707643	0.000000
C	-6.027528	0.751703	0.000000
C	-7.375699	1.238507	0.000000
H	-8.239737	0.611889	0.000000
C	-7.844840	2.523805	0.000000
H	-8.912167	2.776483	0.000000
C	-6.838287	3.426039	0.000000
H	-7.211836	4.432932	0.000000
C	-5.445773	3.061929	0.000000
C	-3.138154	4.132195	0.000000
C	-4.594904	4.233050	0.000000
C	-5.371504	5.444893	0.000000
H	-6.444549	5.489013	0.000000
C	-4.824470	6.680988	0.000000
H	-5.394603	7.617994	0.000000
C	-3.457107	6.631987	0.000000
H	-3.128159	7.647371	0.000000
C	-2.577521	5.500231	0.000000
C	1.028395	0.747173	0.000000
C	-0.392812	1.208951	0.000000
C	3.572865	0.773155	0.000000
C	2.200450	1.598721	0.000000
C	1.839390	3.159078	0.000000
C	0.368762	3.636914	0.000000
C	4.967664	1.498456	0.000000
C	6.205480	0.723793	0.000000
C	7.546065	1.247720	0.000000
H	8.440110	0.652694	0.000000
C	7.830064	2.569281	0.000000
H	8.842070	2.992219	0.000000
C	6.695042	3.333354	0.000000
H	7.025746	4.348167	0.000000

C	5.318213	2.934751	0.000000
C	2.960208	4.261481	0.000000
C	4.434532	4.151033	0.000000
C	5.239089	5.337300	0.000000
H	6.306428	5.338224	0.000000
C	4.863154	6.652882	0.000000
H	5.578119	7.484662	0.000000
C	3.518515	6.791168	0.000000
H	3.228886	7.825328	0.000000
C	2.605967	5.678098	0.000000
C	0.109976	5.187577	0.000000
C	1.229231	6.125426	0.000000
C	1.145210	7.562301	0.000000
H	1.987389	8.228715	0.000000
C	-0.023908	8.240785	0.000000
H	-0.113419	9.333955	0.000000
C	-1.101326	7.397426	0.000000
H	-1.964278	8.025539	0.000000
C	-1.147696	5.964809	0.000000

References

-
- ¹ T. Yani, D. P. Tew, N. C. Handy, *Chem. Phys. Lett.*, 2004, 393, 51-57.
- ² a) W. J. Hehre, R. Ditchfield and J. A. Pople, *J. Chem. Phys.*, 1972, 56, 2257–2261. b) W. J. Hehre, L. Radom, P. V. R. Schleyer and J. A. Pople, *Ab Initio Molecular Orbital Theory*, Wiley, New York, 1986.
- ³ M. J. Frisch, G. W. Trucks, H. B. Schlegel, G. E. Scuseria, M. A. Robb, J. R. Cheeseman, G. Scalmani, V. Barone, B. Mennucci, G. A. Petersson, H. Nakatsuji, M. Caricato, X. Li, H. P. Hratchian, A. F. Izmaylov, J. Bloino, G. Zheng, J. L. Sonnenberg, M. Hada, M. Ehara, K. Toyota, R. Fukuda, J. Hasegawa, M. Ishida, T. Nakajima, Y. Honda, O. Kitao, H. Nakai, T. Vreven, J. A. Montgomery Jr., J. E. Peralta, F. Ogliaro, M. Bearpark, J. J. Heyd, E. Brothers, K. N. Kudin, V. N. Staroverov, R. Kobayashi, J. Normand, K. Raghavachari, A. Rendell, J. C. Burant, S. S. Iyengar, J. Tomasi, M. Cossi, N. Rega, J. M. Millam, M. Klene, J. E. Knox, J. B. Cross, V. Bakken, C. Adamo, J. Jaramillo, R. Gomperts, R. E. Stratmann, O. Yazyev, A. J. Austin, R. Cammi, C. Pomelli, J. W. Ochterski, R. L. Martin, K. Morokuma, V. G. Zakrzewski, G. A. Voth, P. Salvador, J. J. Dannenberg, S. Dapprich, A. D. Daniels, O. Farkas, J. B. Foresman, J. V. Ortiz, J. Cioslowski, D. J. Fox, *Gaussian 09, Revision D.01*, Gaussian, Inc., Wallingford, CT, 2009.
- ⁴ M. Torrent-Sucarrat, S. Navarro, F. P. Cossío, J. M. Anglada, J. M. Luis, *J. Comput. Chem.*, 2017, 38, 2819-2828.
- ⁵ [Submitted on 12 Nov 2020] <https://arxiv.org/pdf/2011.06560.pdf>
- ⁶ J. Kruszewski, T. M. Krygowski, *Tetrahedron Lett.*, 1972, 13, 3839.
- ⁷ H. Fliegl, S. Taubert, O. Lehtonen, D. Sundholm, *Phys. Chem. Chem. Phys.*, 2011, 13, 20500.
- ⁸ P. Bultinck, R. Ponec, S. Van Damme, *J. Phys. Org. Chem.*, 2005, 18, 706.
- ⁹ E. Matito, *Phys. Chem. Chem. Phys.*, 2016, 18, 11839-11846.
- ¹⁰ E. Matito, M. Duran, M. Solà, *J. Chem. Phys.*, 2005, 122, 014109.
- ¹¹ E. Matito, M. Duran, M. Solà, *J. Chem. Phys.*, 2006, 125, 059901.
- ¹² a) D. W. Szczepanik, E. J. Zak, K. Dydych, J. Mrozek, *Chem. Phys. Lett.* 2014, 593, 154–159; b) D. W. Szczepanik, M. Andzejak, K. Dyduch, E. J. Zak, M. Makowski, G. Mazur, J. Mrozek, *Phys. Chem. Chem. Phys.* 2014, 16, 20514–20523; c) D. W. Szczepanik, *Comput. Theor. Chem.* 2016, 1080, 33–37; d) D. W. Szczepanik, *Comput. Theor. Chem.* 2017, 1100, 13–17.
- ¹³ Keith, T. A. AIMAll (Version 14.11.23), TK Gristmill Software: Overland Park KS, USA 2014.
- ¹⁴ E. Matito, M. Solà, P. Salvador, M. Duran, *Faraday Discuss.* 2007, 135, 325-345.
- ¹⁵ E. Matito, P. Salvador, M. Duran, M. Solà, *J. Phys. Chem. A*, 2006, 110, 5108-5113.
- ¹⁶ E. Matito, ESI-3D: Electron Sharing Indexes Program for 3D Molecular Space Partitioning (program available upon request to ematito@gmail.com), Institute of Computational Chemistry and Catalysis, University of Girona, Catalonia, Spain, 2014.
- ¹⁷ A. E. Reed, R. B. Weinhold, *J. Chem. Phys.* 1985, 83, 735–746.
- ¹⁸ E. D. Glendening, J. K. Badenhoop, A. E. Reed, J. E. Carpenter, J. A. Bohmann, C. M. Morales, C. R. Landis, F. Weinhold, NBO 6.0, Theoretical Chemistry Institute, University of Wisconsin: Madison, 2013.
- ¹⁹ M. D. Hanwell, D. E. Curtis, D. C. Lonie, T. Vandermeersch, E. Zurek, G. R. Hutchison, *J. Cheminf.* 2012, 4, 1–17.
- ²⁰ Ahrens, James, Geveci, Berk, Law, Charles, ParaView: An End-User Tool for Large Data Visualization, *Visualization Handbook*, Elsevier, 2005, ISBN-13: 978-0123875822.
- ²¹ D. A. Evans, *Angew. Chem. Int. Ed.* 2014, 53, 11140 – 11145.
- ²² The PyMOL Molecular Graphics System, Version 1.2r3pre, Schrödinger, LLC.
- ²³ Zhurko, G.A. and Zhurko, D.A. Chemcraft. Version 1.7 (<https://www.chemcraftprog.com>).
- ²⁴ T. Heine, C. Corminboeuf, G. Seifert, *Chem. Rev.* 2005, 105, 3889–3910.
- ²⁵ G. Merino, T. Heine, G. Seifert, *Chem. - A Eur. J.* 2004, 10, 4367–4371.
- ²⁶ R. Islas, T. Heine, G. Merino, *Acc. Chem. Res.* 2012, 45, 215–228.
- ²⁷ K. Wolinski, J. F. Hinton, P. Pulay, *J. Am. Chem. Soc.* 1990, 112, 8251–8260.
- ²⁸ G. Schreckenbach, T. Ziegler, *J. Phys. Chem.* 1995, 99, 606–611.
- ²⁹ S. K. Wolff, T. Ziegler, E. van Lenthe, E. J. Baerends, *J. Chem. Phys.* 1999, 110, 7689.
- ³⁰ M. Kaupp, M. Bühl, V. G. Malkin, *Calculation of NMR and EPR Parameters: Theory and Applications*, John Wiley & Sons, Inc., 2006.

-
- ³¹ N. C. Handy, A. J. Cohen, Mol. Phys. 2001, 99, 403–412.
- ³² J. P. Perdew, K. Burke, M. Ernzerhof, Phys. Rev. Lett. 1996, 77, 1396–1396.
- ³³ L. Armangué, M. Solà, M. Swart, J. Phys. Chem. A 2011, 115, 1250–1256.
- ³⁴ M. Baranac-Stojanovic, RSC Adv. 2014, 4, 308–321.
- ³⁵ S. Klod, E. Kleinpeter, J. Chem. Soc. Perkin Trans. 2 2001, 1893–1898.
- ³⁶ N. D. Charistos, A. G. Papadopoulos, M. P. Sigalas, J. Phys. Chem. A 2014, 118, 1113–1122.
- ³⁷ E. Steiner, P. W. Fowler, L. W. Jenneskens, Angew. Chem. Int. Ed. 2001, 40, 362–366.
- ³⁸ A. Kumar, M. Duran, M. Solà, J. Comput. Chem. 2017, 38, 1606–1611.
- ³⁹ M. A. Dobrowolski, M. K. Cyranski, Z. Wróbel, Phys. Chem. Chem. Phys. 2016, 18, 11813–11820.
- ⁴⁰ F. Feixas, E. Matito, J. Poater, M. Solà, J. Phys. Chem. A 2007, 111, 4513–4521.